JOURNAL OF THERMOPHYSICS AND HEAT TRANSFER
Vol. 10, No. 2, April–June 1996

Effects of Freestream Nonequilibrium on Convective Heat Transfer to a Blunt Body

Tahir Gökçen*
NASA Ames Research Center, Moffett Field, California 94035

The axisymmetric Navier–Stokes equations are solved numerically for nonequilibrium airflows over a hemisphere for two sets of conditions. One set corresponds to a wind-tunnel test flow where the freestream is vibrationally excited and dissociated air, and the other corresponds to hypersonic free flight where the freestream is air at atmospheric conditions. Relevant similitude parameters are partially duplicated in the computations as in the wind-tunnel testing of convective heating. A nonequilibrium formulation with a three-temperature thermochemical model has been employed to simulate vibrationally excited and partially dissociated nonequilibrium airflow. Finite catalytic boundary conditions at the surface are implemented. Computations are carried out at enthalpies of 7.2 and 25 MJ/kg, for surface pressures of 0.017 and 0.076 atm, respectively. Computed stagnation point heat transfer is compared with the classical results of Fay and Riddell, and Goulard. The computed results show that successful testing of surface heat transfer in a high-enthalpy tunnel is possible with partial duplication of similitude variables.

Introduction

HIGH-ENTHALPY wind tunnels such as arcjets and shock tunnels are primary means for testing surface heating to a blunt body in hypersonic flight. The characteristics of the flow over a blunt body tested in such a facility are quite different from those in free flight, since a typical test flow is vibrationally excited, partially dissociated and ionized, and in thermochemical nonequilibrium. It is well known that it is impossible to duplicate all flight similitude parameters in ground-based facilities, and therefore, only a partial simulation of the parameters is achieved. For convective heating to the surface of a blunt body, based on the theoretical stagnation point heat transfer studies of Fay and Riddell[1] and Goulard,[2] the most important parameters to be duplicated are total enthalpy, surface pressure, and surface catalytic efficiency.

Using a concept similar to that described earlier, convective heat transfer and pitot pressure at the stagnation point of a blunt body are measured to characterize the test section flow in high-enthalpy wind tunnels.[3–5] From these measurements, total enthalpy of the flow in the test section is deduced using a correlation based on the Fay and Riddell formula with the Goulard correction, which relates stagnation point heat transfer, pitot pressure, and total enthalpy for a given wall catalytic efficiency. A possible source of error in this approach is that several assumptions leading to the Fay and Riddell type correlation (such as undissociated freestream and thermochemical equilibrium at the edge of the boundary layer and thin boundary layer, etc.) are often not satisfied. Furthermore, the arcjet test conditions such as total enthalpy and composition of the gas are not accurately known. These factors make it difficult to determine how well the laboratory environment can simulate the free-flight conditions.

The objective of the present work is to explore the partial simulation concept computationally (i.e., idealized computational arcjet tests). Computations of thermochemical nonequilibrium flows over a hemisphere are carried out for two sets of conditions: one corresponding to a wind-tunnel test flow where the freestream is in a nonequilibrium state; and the other corresponding to the free flight where freestream is air at standard atmospheric conditions. Relevant similitude parameters (the total enthalpy, surface pressure, and catalytic efficiency) are duplicated in computations as in wind-tunnel testing. By comparing these two sets of computations, the effects of freestream nonequilibrium on heat transfer are investigated. Since the accuracy of the computations can be questioned, it is desirable to validate the computational code against theoretical results. Therefore, the flow conditions are chosen such that most of the assumptions leading to the Fay and Riddell theory are approximately valid (low-density effects are not important). The computed heat transfer results can then be validated against the classical results for both catalytic and noncatalytic surfaces.

Formulation

The axisymmetric nonequilibrium formulation of viscous blunt body flows of air is considered. The present formulation employs a thermochemical model with 11 chemical species of air (N_2, O_2, NO, N, O, N_2^+, O_2^+, NO^+, N^+, O^+, e^-), and three internal temperatures (translational, rotational, and vibrational–electronic). The governing Navier–Stokes equations are supplemented with the equations accounting for thermochemical nonequilibrium processes.

Governing Equations

The governing Navier–Stokes equation set for two-dimensional/axisymmetric nonequilibrium airflows can be written in conservation form as

$$\frac{\partial \boldsymbol{U}}{\partial t} + \frac{\partial \boldsymbol{F}}{\partial x} + \frac{1}{y^r}\frac{\partial}{\partial y} y^r \boldsymbol{G} = \boldsymbol{W} + r\boldsymbol{H}/y \tag{1}$$

where $r = 1$ for axisymmetric flows and $r = 0$ for two-dimensional flows. The equation set consists of 16 partial differential equations: 11 mass conservation equations for species, two momentum equations, and three energy equations.

Components of the state vector $\boldsymbol{U}$, the flux vectors $\boldsymbol{F}$ and

Presented as Paper 95-0156 at the AIAA 33rd Aerospace Sciences Meeting and Exhibit, Reno, NV, Jan. 9–12, 1995; received Jan. 23, 1995; revision received Sept. 15, 1995; accepted for publication Nov. 6, 1995.

*Research Scientist, Thermosciences Institute. Member AIAA.

G, the source vectors W for thermochemistry and H for axisymmetric geometry in Eq. (1), are given as follows:

$$U = \begin{bmatrix} \rho_1 \\ \rho_2 \\ \vdots \\ \rho_{11} \\ \rho u \\ \rho v \\ E_v \\ E_r \\ E \end{bmatrix}, \quad F = \begin{bmatrix} \rho_1 u + j_{1x} \\ \rho_2 u + j_{2x} \\ \vdots \\ \rho_{11} u + j_{11x} \\ \rho u^2 + p + \tau_{xx} \\ \rho uv + \tau_{xy} \\ uE_v + q_{vx} \\ uE_r + q_{rx} \\ u(E + p + \tau_{xx}) + v\tau_{xy} + q_x \end{bmatrix}$$

$$G = \begin{bmatrix} \rho_1 v + j_{1y} \\ \rho_2 v + j_{2y} \\ \vdots \\ \rho_{11} v + j_{11y} \\ \rho uv + \tau_{yx} \\ \rho v^2 + p + \tau_{yy} \\ vE_v + q_{vy} \\ vE_r + q_{ry} \\ v(E + p + \tau_{yy}) + u\tau_{yx} + q_y \end{bmatrix} \tag{2}$$

$$W = \begin{bmatrix} w_1 \\ w_2 \\ \vdots \\ w_{11} \\ 0 \\ 0 \\ w_v \\ w_r \\ 0 \end{bmatrix}, \quad H = \begin{bmatrix} 0 \\ 0 \\ \vdots \\ 0 \\ 0 \\ p + \tau_{\theta\theta} \\ 0 \\ 0 \\ 0 \end{bmatrix}$$

The diffusive fluxes in F and G are computed using the linear transport laws, i.e., the Navier–Stokes diffusion of momentum, Fourier's law of heat conduction, and Fick's law of mass diffusion.

The species viscosity and heat conductivity are computed from the curve fits of Gupta et al.[6] For mass diffusion, three diffusion coefficients are used: 1) one for all neutral species, 2) one for all ionic species, and 3) one for electrons. The neutral species diffusion coefficient is calculated assuming a constant Schmidt number of 0.5, and ambipolar diffusion is assumed for ionic species. The diffusion coefficient of electrons is computed as the average diffusion velocity of ions.

Components of the source vector W for the 11-species thermochemical model have been described in detail in the literature.[7,8] Although rotational nonequilibrium is allowed in the formulation, translational and rotational energy modes are assumed to be in equilibrium, and the two-temperature model of Park[9] for the reactions and rate coefficients is employed. Previous applications of this formulation and thermochemical model are reported in Refs. 10 and 11.

Numerical Method

The governing equations are discretized using a finite volume approach and the resulting difference equations are solved using an implicit Gauss–Seidel relaxation method.[12] The convective fluxes are approximated using a Steger–Warming type flux vector splitting. Second-order accuracy is achieved through a variable interpolation, except near the shock wave. The viscous fluxes are approximated by central differencing. The numerical method is fully implicit for fluid dynamics and thermochemistry.

Finite catalytic boundary conditions for species mass fractions at the surface are implemented, and no-slip conditions for the velocity and constant wall temperature are prescribed.

Catalytic Wall Boundary Conditions

Solid walls play a catalytic role in the chemical reactions that involve the recombination of atoms. Therefore, the prediction of the convective heat transfer to the wall, when the flow is in thermochemical nonequilibrium, must account for surface catalysis. It is well known that the heat transfer to a solid surface is extremely sensitive to the wall catalycity, provided that the flow is in a nonequilibrium state and it includes dissociated atoms.[13,14]

Catalytic wall boundary conditions are obtained by balancing the mass flux of species with the chemical rate of production or depletion caused by surface reactions. For an impermeable wall, this balance is described by

$$j_{in} + R_i = 0 \tag{3}$$

where j_{in} is the diffusive flux of species i, and R_i is the rate of depletion of species i caused by surface reactions. The rate R_i needs to be determined from studies of the chemical kinetics of heterogeneous reactions and analysis of gas–surface interaction. The treatment of the catalytic wall boundary conditions follows the work in Ref. 12. A comprehensive review on the subject is given by Ref. 15.

For most aerospace applications the surface temperature is low enough (e.g., 1000 K) that the recombination of dissociated atoms is the only dominant chemical process occurring at the surface. The surface recombination reaction is assumed to be a first-order reaction such that $R_i = k_{w_i}\rho_i$. The rate constant k_{w_i} is described by a phenomenological model as $k_{w_i} = \gamma_i\sqrt{\bar{R}T_w/2\pi M_i}$, where γ_i is the catalytic efficiency of the wall and represents the fraction of atoms that recombine upon colliding with the surface.

For the current 11-species air model, it is assumed that the surface is noncatalytic for NO and all ionic species and only the recombination reactions of atomic species are significant in the wall collisions. Although the noncatalytic wall condition for ion recombination reactions may not be a good physical model in general, it is justified here for dissociation-dominated flows (i.e., ionization levels are small).

Thus, the surface reactions of interest are

$$N + N \xrightarrow{\gamma_N} N_2, \qquad O + O \xrightarrow{\gamma_O} O_2$$

The surface reaction rates for the atomic species are

$$R_N = k_{w_N}\rho_N, \qquad R_O = k_{w_O}\rho_O \tag{4}$$

Rates for diatomic species are described by

$$R_{N_2} = -R_N, \qquad R_{O_2} = -R_O, \qquad R_{NO} = 0 \tag{5}$$

In the present formulation, noting that the diffusive fluxes of species are given by

$$j_{in} = -\rho D\frac{\partial c_i}{\partial n} \tag{6}$$

the catalytic boundary conditions are specified for neutral species by

$$\frac{\partial c_{N_2}}{\partial n} = -K_N c_N, \qquad \frac{\partial c_{O_2}}{\partial n} = -K_O c_O, \qquad \frac{\partial c_{NO}}{\partial n} = 0$$

$$\frac{\partial c_N}{\partial n} = K_N c_N, \qquad \frac{\partial c_O}{\partial n} = K_O c_O \tag{7}$$

where $K_i = k_{w_i}/D$. For all ionic species the wall is assumed to be noncatalytic, such that $\partial c_i/\partial n = 0$.

The terms fully catalytic and noncatalytic are used loosely in the literature to indicate the degree of wall catalycity. To avoid ambiguity here, these terms are defined with respect to the catalytic efficiency γ_i. The wall is referred to as noncatalytic and fully catalytic when γ_i is zero and unity, respectively. Even though the catalytic efficiencies of the wall are unity, the mass fraction of atomic species at the wall may not be zero, since the chemical reactions on the surface occur at a finite rate. Specification of zero concentrations of the atomic species for a fully catalytic wall is appropriate only if the surface reactions occur at an infinite rate.

Heat Transfer in a Nonequilibrium Flow

In a nonequilibrium flow, the heat flux at the wall is composed of conduction and diffusion components:

$$q_w = -\kappa_t \frac{\partial T}{\partial n} - \kappa_r \frac{\partial T_r}{\partial n} - \kappa_v \frac{\partial T_v}{\partial n} - \sum \rho D \frac{\partial c_i}{\partial n} h_i \qquad (8)$$

In a dissociated blunt body flow, the importance of the diffusion component of heat transfer varies significantly depending on wall catalycity and the thermodynamic state of the gas in the boundary layer. The conditions under which the boundary layer is in an equilibrium, frozen, or nonequilibrium state is determined by the Damköhler number (recombination parameter) associated with gas-phase reactions.[1,2] By definition, when the time scale of gas-phase chemical reactions is large compared to the time scale of the flow, the flow is said to be chemically frozen.

When the boundary layer is frozen to chemical reactions, the wall catalycity has the greatest effect on the surface heat transfer. Since in a frozen boundary layer the time scale for recombination reactions is small compared to the diffusion time, the catalaytic wall reaction is the only mechanism to transport the chemical energy of atoms to the wall by diffusion. On the other hand, in an equilibrium boundary layer, dissociated atoms recombine via gas-phase reactions and the chemical energy is converted to internal energy within the boundary layer. In this situation, the wall catalycity has very little effect on the heat transfer. The concentration of atomic species at the wall is then determined by the equilibrium value corresponding to the wall temperature and pressure and would be essentially zero for a cold wall.

Classical Heat Transfer Correlations

Most correlations for convective heating to a blunt body in dissociated flows are based on the classical theory of Fay and Riddell[1] and their numerical solution of stagnation point boundary-layer equations. Therefore, with reference to Fig. 1, a summary of the conditions for the theory to be applicable here is:

1) The flowfield can be divided into a separate shock layer and boundary layer (not a merged layer).

2) Thermochemical equilibrium is reached at the edge of the boundary layer.

3) The thermochemical state of the gas in the viscous boundary layer is idealized to be either chemically frozen or in equilibrium.

4) The effect of wall catalycity is idealized to be either a fully catalytic wall with infinitely fast reactions or a noncatalytic wall.

5) The shock stand-off distance is large compared to boundary-layer thickness so that viscous vorticity interactions are not important.

6) The air is a binary mixture of atoms and molecules and the Prandtl number Pr and Lewis number Le are assumed to be constant in the boundary layer.

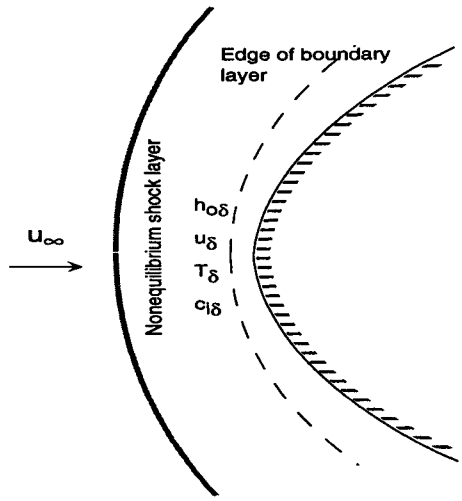

Fig. 1 Sketch of nonequilibrium blunt body flow.

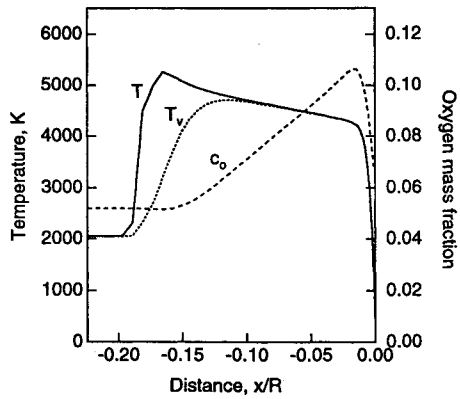

Fig. 2 Stagnation streamline profiles for the flow over a hemispherical probe of 0.476 cm radius.

Fay and Riddell give the following expression for fully catalytic wall (with infinitely fast reactions):

$$q_{k_w=\infty} = 0.763 Pr^{-0.6} (\rho_\delta \mu_\delta)^{0.4} (\rho_w \mu_w)^{0.1} \sqrt{\left(\frac{du_\delta}{dx}\right)_s} \times (h_{o\delta} - h_w) \left[1 + (Le^n - 1)\left(\frac{h_D}{h_{o\delta}}\right)\right] \qquad (9)$$

where h_D is energy in dissociation, subscript w refers to the wall, subscript δ to the edge of the boundary layer, and the exponent n is 0.52 and 0.63 for equilibrium and frozen boundary layers, respectively. By noting that Le is of order unity for air, it can be deduced from Eq. (9) that heat flux to the surface is fairly independent of the flowfield thermochemistry as long as the recombination of atoms is completed at the wall.

Goulard[2] allowed catalytic wall reactions to proceed at a finite speed (removal of restriction 4) and expressed the relative effect of finite wall reactions through a correction parameter. Goulard gives the following expression for heat transfer compared to the heat transfer with infinitely fast reactions:

$$\bar{q} = q/q_{k_w=\infty} = 1 - \frac{Le^{2/3} h_D/h_{o\delta}}{1 + (Le^{2/3} - 1) h_D/h_{o\delta}} (1 - \varphi) \qquad (10)$$

where φ is the Goulard parameter given by

$$\varphi = 1 \Big/ \left[1 + 0.47 Sc^{-2/3} \left(2\rho_\delta \mu_\delta \frac{du_\delta}{dx}\right)^{1/2} \Big/ (\rho_w k_w)\right] \qquad (11)$$

Table 1 Surface pressure and freestream conditions for 7.2-MJ/kg enthalpy cases

Parameter	Free flight	Arcjet tunnel
h_0, MJ/kg	7.2	7.2
p_s, atm	0.0168	0.0168
u_∞, m/s	3750	2780
p_∞, Pa	8.188	1.403×10^2
ρ_∞, kg/m^3	1.296×10^{-4}	2.267×10^{-4}
T_∞, K	220	2050
$T_{v\infty}$, K	220	2050
$c_{N_2\infty}$	0.7381	0.7637
$c_{O_2\infty}$	0.2619	0.1443
$c_{NO\infty}$	0	0.0670
$c_{N\infty}$	0	0
$c_{O\infty}$	0	0.0520

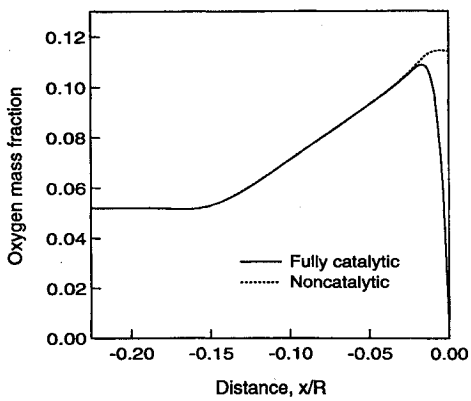

Fig. 3 Oxygen mass fraction along the stagnation streamline of the arcjet blunt body flow.

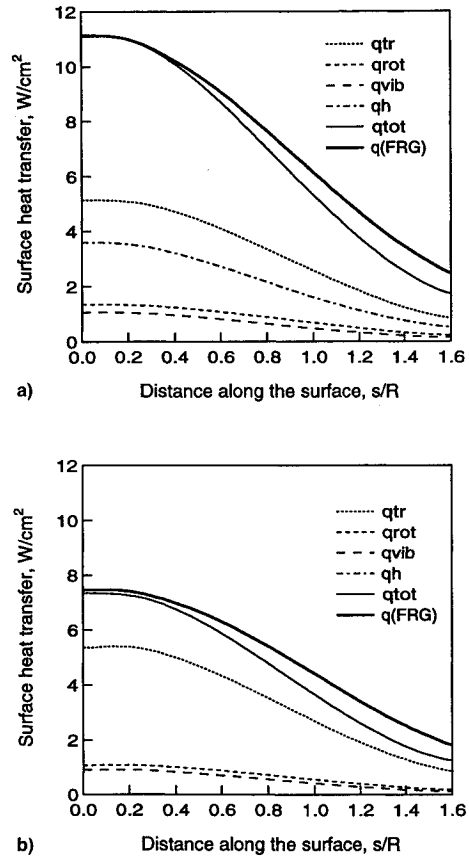

Fig. 4 Comparison of computed heat transfer for the arcjet flow with the Fay and Riddell theory: a) fully catalytic surface (γ_N = γ_O = 1) and b) noncatalytic surface (γ_N = γ_O = 0).

The effect of finite catalytic reaction rates can be stated as follows: for a given surface material, the heat transfer by catalysis increases with velocity, nose radius, and wall temperature and decreases with altitude. Therefore, for higher altitudes or lower densities the effect of the Goulard correction becomes significant.

For practical application of Eqs. (9–11), the velocity gradient and transport properties of the dissociated gas at the edge of the boundary layer must be known. The transport properties are computed using the pressure and temperature obtained from equilibrium shock relations. The velocity gradient at the edge of the boundary layer near the stagnation point is usually estimated from the stagnation point flow and the Newtonian theory, and within the classical hypersonic flow approximation it is given by

$$\left(\frac{du_\delta}{dx}\right)_s = \frac{1}{R}\sqrt{\frac{2(p_\delta - p_\infty)}{\rho_\delta}} \tag{12}$$

Presentation of Results

Two sets of axisymmetric blunt body flows with nonequilibrium thermochemistry are computed at enthalpies of 7.2 and 25 MJ/kg, for surface pressures of 0.017 and 0.076 atm, respectively. An effort was made in choosing the freestream conditions such that the idealized conditions of the Fay and Riddell, and the Goulard theory are approximately satisfied. Freestream conditions and geometry must be such that there is a distinct shock layer and boundary layer, an equilibrium region behind the shock, and a chemically frozen boundary layer. Unfortunately, these conditions are very restrictive with the current thermochemical model and a realistic geometry.

All computations presented here used a 60 × 80 grid (80 points normal to the wall). Since the computed heat transfer at the stagnation point using the 60 × 80 grid was within 1.5% of that using a 40 × 40 grid, it was concluded that the number of points was sufficient to resolve the shock layer and the boundary layer for the purpose of heat transfer computations.

7.2-MJ/kg Enthalpy Cases

The 7.2 MJ/kg enthalpy case is chosen from an actual test condition at a NASA Ames arcjet facility. The freestream conditions are obtained from a nonequilibrium flow computation through an arcjet nozzle using the code described in Ref. 16. The flow over a spherical heat transfer probe of 0.476 cm radius is computed. This case is chosen because the total enthalpy is relatively low such that O_2 dissociation and vibrational relaxation are the only important nonequilibrium processes.

In Fig. 2, temperature and oxygen mass fraction along the stagnation streamline are plotted for noncatalytic wall boundary conditions. Even though the noncatalytic wall boundary conditions are prescribed, it is evident from the variation of oxygen mass fraction that the flow is in a nonequilibrium state, and that the boundary layer is not frozen to oxygen recombination. To establish a frozen boundary-layer flow, the freestream density of the gas is decreased and the nose radius is increased in a manner to keep the binary scaling factor $\rho_\infty R$ constant. By decreasing the density in this way, the boundary layer becomes chemically frozen since the recombination reaction is a three-body reaction, while flowfield chemistry behind the shock is kept similar. For conditions prescribed, the nose radius of 1 m was sufficient to establish a frozen boundary-layer flow.

Once the freestream conditions necessary to have a frozen boundary layer are established, computations are carried out corresponding to the arcjet wind tunnel and free-flight cases with various catalytic wall boundary conditions. The surface pressure and freestream conditions for 7.2-MJ/kg enthalpy cases with 1-m-radius hemisphere are given in Table 1. The equivalent freestream conditions for the free-flight case are

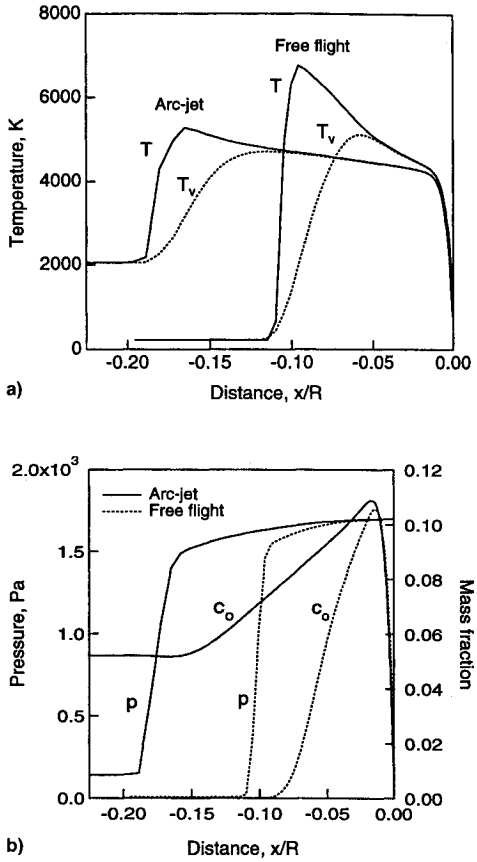

Fig. 5 Approximate matching of flow properties along the stagnation streamline: a) temperature and b) pressure and oxygen mass fraction profiles.

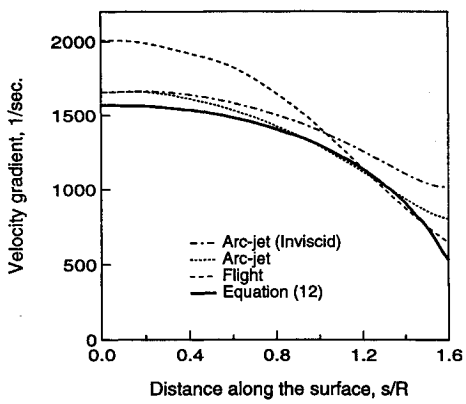

Fig. 6 Comparison of velocity gradients at the edge of boundary layer.

determined such that total enthalpy of the flow and the surface pressure are approximately duplicated. The flight condition corresponds to that of approximately 67-km Earth altitude.

For the arcjet blunt body flow, computed oxygen mass fraction profiles using fully catalytic and noncatalytic boundary conditions are presented in Fig. 3. The difference in the oxygen mass fraction in the boundary layer near the wall is entirely because of wall catalysis.

In Fig. 4, computed surface heat transfer is compared against the classical results of Fay and Riddel and of Goulard (labeled FRG) given by Eqs. (9–11). The transport properties and velocity gradient at the edge of the boundary layer in Eqs. (9–11) are determined from the computed flowfield. The edge of the boundary layer is arbitrarily taken as the location where the total enthalpy does not vary more than 0.5% between adjacent grid points and is within 1% of freestream total enthalpy.

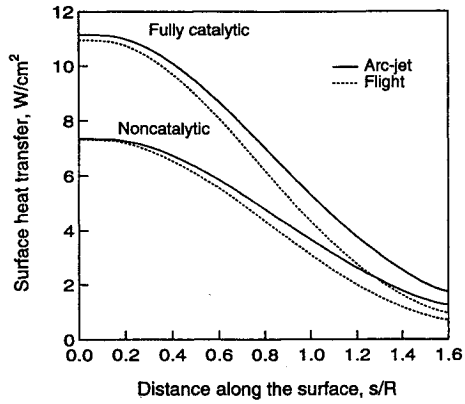

Fig. 7 Comparison of fully catalytic and noncatalytic heat fluxes for the arcjet flow and free flight.

For both catalytic and noncatalytic cases, the computed heat transfer results agree with the classical results, particularly in the stagnation region. Although strict comparison is only valid at the stagnation region, for a given velocity gradient and flow properties at the edge of boundary layer, Eqs. (9–11) can be used to compute surface heat transfer away from the stagnation point (assuming that boundary-layer profiles are self-similar). This is a good validation case because most of the assumptions leading to the Fay and Riddell theory are valid: the flow at the edge of the boundary layer is not far from thermochemical equilibrium; the boundary layer is chemically frozen; and the shock stand-off distance is large enough that the boundary-layer displacement and the vorticity interaction effects are not significant. In Fig. 4, the separate contributions of the conduction (translation, rotation, and vibration) and diffusion components of the computed heat flux are also presented. The diffusive heat flux q_h is a significant portion of the total heat flux when a fully catalytic surface is used. Also, note that the diffusive flux to the surface is eliminated when a noncatalytic surface is used since the boundary layer is chemically frozen.

For the prescribed conditions, the flow properties at the edge of the boundary layer of the arcjet flow and free-flight match approximately. In Fig. 5, the stagnation streamline profiles of both cases using fully catalytic wall conditions are shown. Note that flow structures are noticeably different in the shock layer and are fairly similar in the boundary layer. The dissociated and vibrationally excited freestream of the arcjet flow results in a much larger shock stand-off distance than that in the free-flight case. Also, since the flow has not reached chemical equilibrium at the edge of the boundary layer, there is a small difference in atomic oxygen levels.

It is well known that velocity gradient has an important effect on convective heat transfer. In Fig. 6, the computed velocity gradients at the edge of boundary layer for both the arcjet flow and free flight, the computed velocity gradient at the surface for the inviscid arcjet flow, and the value computed from Eq. (12) are presented. Note that Eq. (12) underestimates the velocity gradient compared to both viscous and inviscid computations. As expected, the difference in velocity gradients for the arcjet flow and free flight is caused by the difference in shock stand-off distances.

Computed total heat fluxes for the arcjet flow and free-flight cases are compared in Fig. 7. By simply duplicating the total enthalpy and surface pressure for both fully catalytic and noncatalytic surfaces, the surface convective heating is simulated satisfactorily, particularly near the stagnation point. It is not clear why the fully catalytic heat flux for the free flight is slightly lower than the arcjet heat flux in spite of the higher velocity gradient at the edge of boundary layer. It may be that there is less dissociated oxygen at the edge of the boundary layer, and therefore, less energy present in the chemical mode to transfer to the wall by diffusion.

Table 2 Surface pressure and freestream conditions for 25-MJ/kg enthalpy cases

Parameter	Free flight	Arcjet tunnel
h_0, MJ/kg	25.21	25.05
p_s, atm	0.0758	0.0762
u_∞, m/s	7070	5630
p_∞, Pa	10.11	96.12
ρ_∞, kg/m^3	1.600×10^{-4}	2.546×10^{-4}
T_∞, K	220	970
$T_{v\infty}$, K	220	2800
$c_{N_2\infty}$	0.7381	0.6274
$c_{O_2\infty}$	0.2619	0
$c_{NO\infty}$	0	0
$c_{N\infty}$	0	0.1104
$c_{O\infty}$	0	0.2622

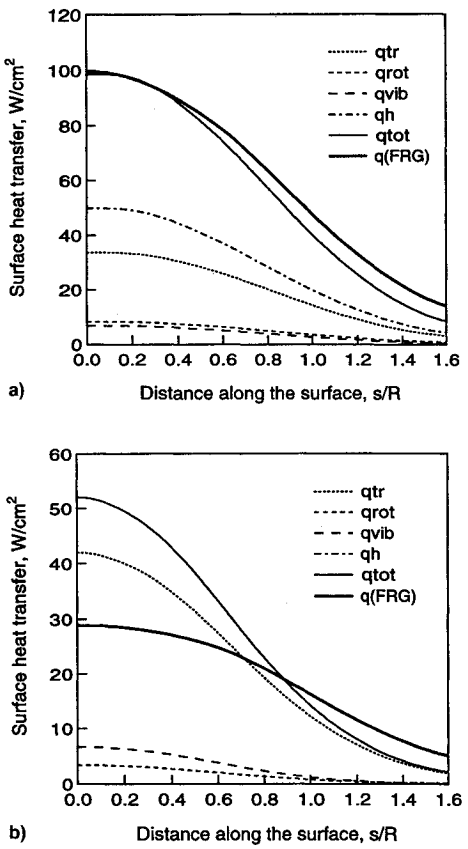

Fig. 8 Comparison of computed heat transfer for an arcjet flow with the Fay and Riddell theory: a) fully catalytic surface (γ_N = γ_O = 1) and b) noncatalytic surface (γ_N = γ_O = 0).

25-MJ/kg Enthalpy Cases

The second set of computations of flow over a hemisphere of radius 1 m are made at a relatively high enthalpy of 25 MJ/kg, where all of the oxygen and a significant portion of the nitrogen are dissociated behind the shock. For the arcjet flow, the freestream is in a dissociated and vibrationally frozen state. Again, the equivalent freestream conditions for free flight are determined such that total enthalpy of the flow and the surface pressure are duplicated approximately. The flight condition corresponds to that of approximately 65-km Earth altitude. The surface pressure and freestream conditions are summarized in Table 2.

In Fig. 8, computed heat transfer results for the arcjet flow using fully catalytic and noncatalytic boundary conditions are compared with the Fay and Riddell theory. The conduction and diffusion components of the heat flux are also shown. Note that the diffusion component at the stagnation point is almost 50% of the total flux for the catalytic case. The computations

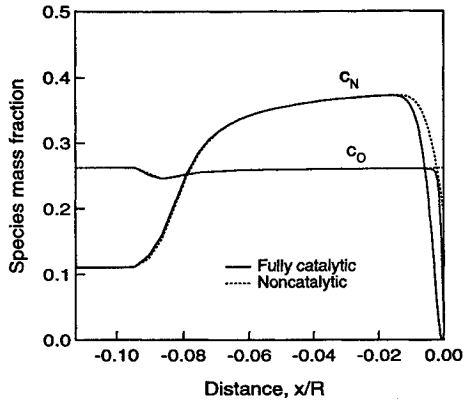

Fig. 9 Computed species mass fraction for fully catalytic and noncatalytic wall conditions.

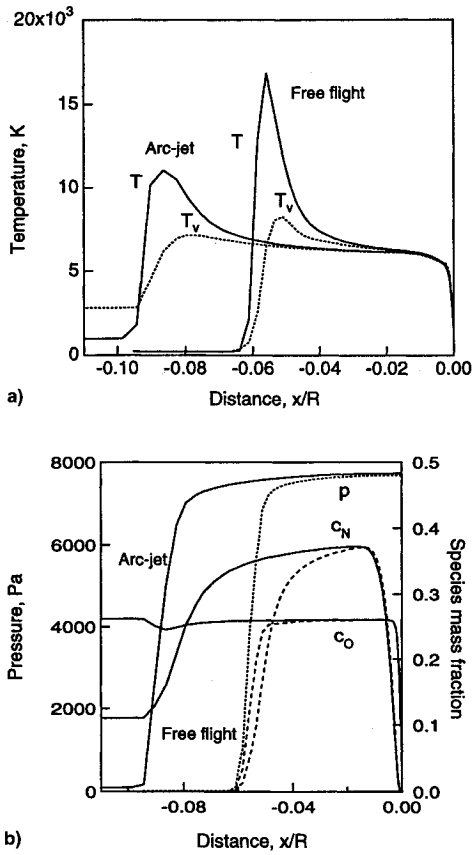

Fig. 10 Approximate matching of flow properties along the stagnation streamline for fully catalytic wall (γ_N = γ_O = 1): a) temperature and b) pressure and species mass fraction profiles.

are in good agreement with the theory for a fully catalytic surface, but not so for a noncatalytic surface. The reason for this discrepancy is that the boundary-layer flow is not frozen to nitrogen recombination, which is assumed by the Fay and Riddell theory. Consequently, some of the energy present in the chemical mode of the dissociated nitrogen atoms is transferred to internal energy modes by recombination and is then conducted to the surface. It should be pointed out that, as seen from Fig. 8b, when the boundary layer is not frozen, the reduction in the heat transfer because of the noncatalytic wall is much less than what the classical theory predicts.

Profiles of atomic species mass fractions along the stagnation streamline of the arcjet flow for fully catalytic and noncatalytic wall conditions are shown in Fig. 9. For noncatalytic conditions, it is evident that nitrogen recombination in the

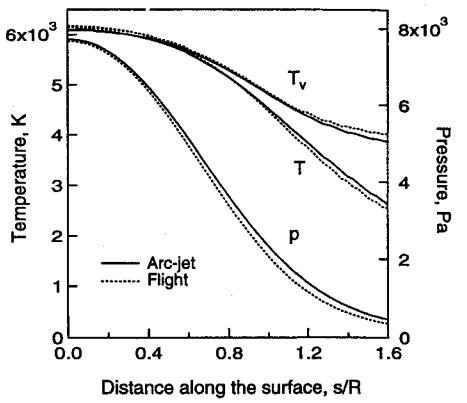

Fig. 11 Comparison of temperatures and pressure at the edge of the boundary layer.

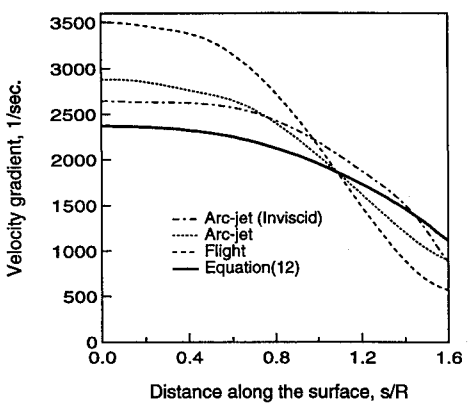

Fig. 12 Comparison of velocity gradients at the edge of the boundary layer.

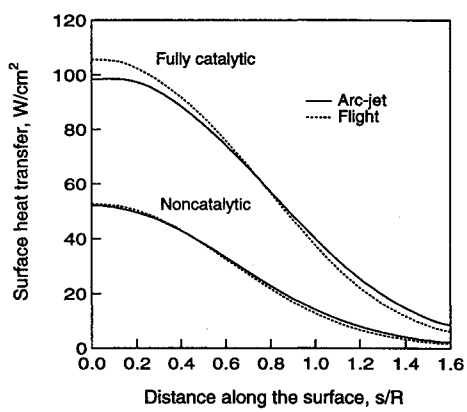

Fig. 13 Comparison of computed fully catalytic and noncatalytic heat fluxes for the arcjet flow and free flight.

boundary layer is taking place while oxygen recombination is frozen.

For the arcjet flow and free flight, stagnation streamline profiles of temperature, pressure, and mass fractions of atomic species are presented in Fig. 10. Temperatures and pressure at the edge of the boundary layer are compared throughout the flowfield in Fig. 11. Good matching of flow properties is observed since the flow at the edge of the boundary layer is close to the thermochemical equilibrium.

In Fig. 12, velocity gradients at the edge of boundary layer are compared against the inviscid velocity gradient at the surface and the computed values from Eq. (12). Because of the difference in shock stand-off distances, there is a difference in the velocity gradient at the edge of boundary layer, similar to that observed in the low-enthalpy case. However, even for the arcjet flow, the effect of boundary-layer displacement on the

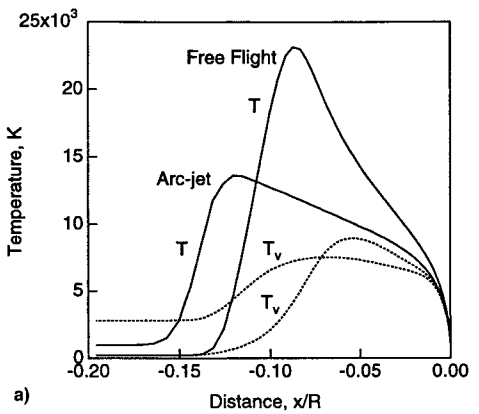

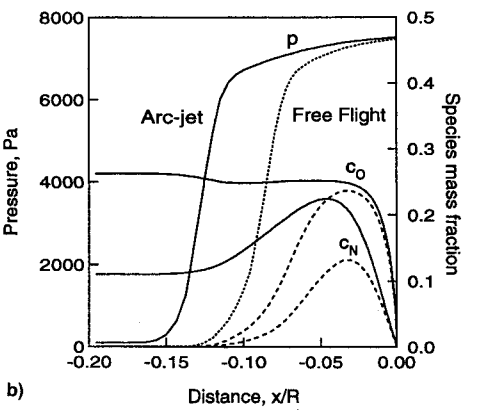

Fig. 14 Computed flow properties for arcjet and free-flight conditions along the stagnation streamline of a 5.08-cm-radius hemisphere: a) temperature and b) pressure and species mass fraction profiles.

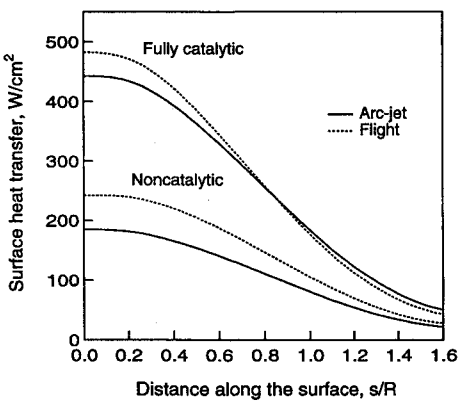

Fig. 15 Comparison of computed fully catalytic and noncatalytic heat fluxes for the free flight and arcjet flow over a 5.08-cm-radius hemisphere.

velocity gradient is apparent since the boundary-layer thickness is no longer negligible compared to the shock stand-off distance. Again, Eq. (12) underestimates significantly the velocity gradient and this discrepancy becomes larger as the shock stand-off distance gets smaller.

Comparison of the computed fully catalytic and noncatalytic heat fluxes for the arcjet flow and free-flight cases is presented in Fig. 13. Again the agreement is very satisfactory. Clearly, this comparison shows that as long as the flow properties at the edge of boundary layer are matched, the surface heat transfer is reproduced, and the effect of flowfield features is in fact a second-order effect.

The flow computations at 25 MJ/kg enthalpy are repeated for a hemisphere of 5.08 cm radius for which the assumption

of the thermochemical equilibrium at the boundary-layer edge is not satisfied. For the arcjet flow and free flight, stagnation streamline profiles of temperature, pressure, and mass fractions of atomic species are presented in Fig. 14. It is clear that the flow properties at the boundary-layer edge do not match since thermochemical equilibrium is not reached. Consequently, at the edge of boundary layer, distribution of the enthalpy in various modes, internal and chemical modes, are significantly different for arcjet flow and free flight.

The computed heat fluxes for fully catalytic and noncatalytic walls are presented in Fig. 15. For a fully catalytic wall case, the agreement between arcjet and free flight is still reasonably good. This result might be expected since Lewis number for air is order of unity. On the other hand, for a noncatalytic wall case, the heat flux for free flight is significantly larger than that for the arcjet flow. The reason is that, as observed in Fig. 14, the internal energy component of the free-flight enthalpy at the boundary-layer edge is much larger than that of the arcjet flow. The noncatalytic heat flux is sensitive to thermodynamic state of the gas in the boundary layer and the degree of nonequilibrium at the boundary-layer edge. Note that for these conditions the classical theory cannot be used to predict the surface heat transfer.

Concluding Remarks

Viscous axisymmetric flows of vibrationally excited and partially dissociated nonequilibrium air over a hemisphere are computed for two sets of conditions using a two-temperature thermochemical model. One set corresponds to a wind-tunnel test flow where the freestream is vibrationally excited and dissociated air, and the other corresponds to the hypersonic free flight where freestream is air at atmospheric conditions. Computed surface heat transfer is compared with the classical results of Fay and Riddell, and of Goulard. Good agreement is obtained when the conditions leading to the Fay and Riddell theory are applicable. The computed results show that successful testing of surface heat transfer in an arcjet environment is possible by the partial duplication of similitude variables (total enthalpy, surface pressure, and wall catalycity) when the certain conditions are satisfied. For fully catalytic surfaces, partial duplication of enthalpy and pressure provides adequate simulation. For noncatalytic surfaces, the thermochemical equilibrium at the edge of the boundary layer appears to be a very important requirement for successful testing. The noncatalytic heat flux is significantly affected by the thermodynamic state of the gas in the boundary layer and degree of nonequilibrium at the boundary-layer edge. In actual arcjet flow environments where the Fay and Riddell theory is no longer applicable, a validated CFD code should be used to interpret surface heat transfer measurements.

Acknowledgments

Support from the Reacting Flow Environments Branch at NASA Ames Research Center through Grant NCC2-452 to Eloret Institute and Contract NAS2-14031 to Eloret is gratefully acknowledged. The author would also like to thank Chul Park for his suggestions and informative discussions.

References

[1]Fay, J. A., and Riddell, F. R., "Theory of Stagnation Point Heat Transfer in Dissociated Air," *Journal of the Aerospace Sciences*, Vol. 25, No. 2, 1958, pp. 73–85.

[2]Goulard, R., "On Catalytic Recombination Rates in Hypersonic Stagnation Heat Transfer," *Jet Propulsion*, Vol. 28, No. 11, 1958, pp. 733–745.

[3]Pope, R. B., "Measurements of Enthalpy in Low-Density Arc-Heated Flows," *AIAA Journal*, Vol. 6, No. 1, 1968, pp. 103–110.

[4]Folck, J. L., and Smith, R. T., "Hypersonic Flow Diagnostic Studies in a Large Arc-Heated Wind Tunnel," *AIAA Journal*, Vol. 8, No. 8, 1970, pp. 1470–1476.

[5]Scott, C. D., "Survey of Measurements of Flow Properties in Arcjets," *Journal of Thermophysics and Heat Transfer*, Vol. 7, No. 1, 1993, pp. 9–24.

[6]Gupta, R. N., Yos, J. M., Thompson, R. A., and Lee, K. P., "A Review of Reaction Rates and Thermodynamic and Transport Properties for an 11-Species Air Model for Chemical and Thermal Nonequilibrium Calculations to 30,000 K," NASA-RP 1232, Aug. 1990.

[7]Park, C., *Nonequilibrium Hypersonic Aerothermodynamics*, Wiley, New York, 1989.

[8]Gnoffo, P. A., Gupta, R. N., and Shinn, J. L., "Conservation Equations and Physical Models for Hypersonic Air Flows in Thermal and Chemical Nonequilibrium," NASA TP-2867, Feb. 1989.

[9]Park, C., "Review of Chemical-Kinetic Problems of Future NASA Missions, Part I: Earth Entries," *Journal of Thermophysics and Heat Transfer*, Vol. 7, No. 3, 1993, pp. 385–398.

[10]Gökçen, T., "Computation of Nonequilibrium Radiating Shock Layers," AIAA Paper 93-0144, Jan. 1993.

[11]Boyd, I. D., and Gökçen, T., "Computation of Axisymmetric and Ionized Hypersonic Flows Using Particle and Continuum Methods," *AIAA Journal*, Vol. 32, No. 9, 1994, pp. 1828–1835.

[12]Gökçen, T., "Computation of Hypersonic Low Density Flows with Thermochemical Nonequilibrium," Ph.D. Dissertation, Stanford Univ., Stanford, CA, June 1989.

[13]Pope, R. B., "Stagnation-Point Convective Heat Transfer in Frozen Boundary Layers," *AIAA Journal*, Vol. 6, No. 4, 1968, pp. 619–626.

[14]Anderson, L. A., "Effect of Surface Catalytic Activity on Stagnation Heat-Transfer Rates," *AIAA Journal*, Vol. 11, No. 5, 1973, pp. 649–656.

[15]Scott, C. D., "Wall Catalytic Recombination and Boundary Conditions in Nonequilibrium Hypersonic Flows with Applications," *Advances in Hypersonic, Vol. 2: Modeling Hypersonic Flows*, edited by J. J. Bertin, J. Périaux, and J. Ballmann, Birhäuser, Boston, 1992, pp. 176–250.

[16]Gökçen, T., "Computation of Nonequilibrium Viscous Flows in Arc-Jet Wind Tunnel Nozzles," AIAA Paper 94-0254, Jan. 1994.